The 2009 IEEE/RSJ International Conference on
Intelligent Robots and Systems
October 11-15, 2009 St. Louis, USA

Development of a 6-DOF Manipulator Actuated with a Straight-Fiber-Type Artificial Muscle

Hiroyuki Maeda,* Hidekazu Nagai,* and Taro Nakamura*

*Chuo University
Faculty of Science and Engineering, Department of Precision Mechanics,
1-13-27 Kasuga, Bunkyou-ku, Tokyo 112-8551, JAPAN
nakamura@mech.chuo-u.ac.jp

Abstract—**Robots have become an integral part of human life, and the relationship between humans and robots has grown closer. Thus, it is desired that robots have characteristics similar to humans. In this context, we paid attention to an artificial muscle actuator. We used straight-fiber-type artificial muscles, derived from the McKibben type, which have excellent characteristics with respect to the contraction rate and force. We developed a 6-DOF manipulator actuated by a straight fiber artificial muscle. Furthermore, we tried to control the manipulator position by considering its characteristics.**

Index Terms **Straight-fiber-type artificial muscle, 6-DOF manipulator, Inverse kinematics, Position control.**

I. Introduction

Robots are common in various fields, such as medical treatment, nursing, and as mechanical pets. There is a high probability that robots will come into even greater interaction with humans in future. Therefore, there is an increased need for safety with regards to robot–human interaction, as well as for suitable operating performance when collaborating with humans.

We studied straight-fiber-type artificial muscles [1] as robot actuators. This type of artificial muscle has a greater contraction ratio and power than the conventional McKibben-type muscles [2–6]. These muscles are extremely lightweight and flexible, giving greater drivable range and torque to a manipulator made of straight-fiber-type artificial muscle. Furthermore, the muscles also have high compliance. The manipulator can assure safe operation during robot–human interaction and thus, seems suitable for collaborating in human activities.

However, the muscles have nonlinear characteristics and the position control tends to be unstable. As this manipulator does not use gears, position control can be affected adversely by load torque, thus making it difficult to control the artificial muscle.

In this study, we developed a 6-DOF manipulator, consisting of a shoulder, an elbow, and wrist joints, based on human arm. In addition, we also introduced a mechanical equilibrium model [7–8] for the artificial muscle manipulator. This method provides more stable control than the conventional PI control, and can control joint stiffness that affects the inertial and load torque.

This paper consists of five sections. In the second section, we explain the straight fiber artificial muscle. In the third section, we outline the development of the 6-DOF manipulator and controller. The fourth section shows experimental results for the positional control of the manipulator. We offer our conclusions in the fifth section.

II. Straight-fiber-type Artificial Muscle

A. Outline of the Artificial Muscle

Fig. 1 shows a schematic diagram of the straight-fiber-type artificial muscle. The tube, shown in this figure, is made from natural latex rubber with glass fibers fixed at either end by a terminal inserted in the long-axis direction.

Since glass fiber of the muscle suppresses the axial expansion, the muscle expands radially with air pressure and exerts a contractile force axially. In addition, the ring installed in the muscle prevents an explosion due to excessive expansion, and its influence can be modified by adjusting the ratio between the length and radius of the muscle under different conditions.

B. Pressure Characteristics of the Artificial Muscle

Fig. 2 shows the pressure characteristics of the straight-fiber-type artificial muscle. The muscle length is represented l_0 and its contraction as x. As shown in the figure, muscle contraction can be controlled with the pressure characteristics, and the muscle can be used as an actuator. However, the muscle pressure characteristics are highly nonlinear and have strong hysteresis due to the material used. These characteristics affect the manipulator position control.

C. Compliance of the Artificial Muscle

Since the straight-fiber-type artificial muscle has compliance, safety can be assured during manipulator–human contact. However, compliance introduces instability in position control. Therefore, we can control the effect of inertial and load torque by control compliance.

Fig. 3 shows the load characteristics, i.e., the relationship between the displacement and load. In this figure the pressure is related to the load characteristics, and compliance can be regarded as linear for small displacements (0–40 mm). Therefore, we consider that compliance can be controlled with pressure. Fig. 4 shows the artificial muscle stiffness for each pressure value, where the relationship between pressure and stiffness is almost proportional. Therefore, the stiffness is expressed by the equation

$$k = k_a P, \quad (1)$$

where, the artificial muscle stiffness is k, the pressure exerted on the artificial muscle P, and the stiffness characteristic constant $k_a = 37.6 \times 10^{-9}$.

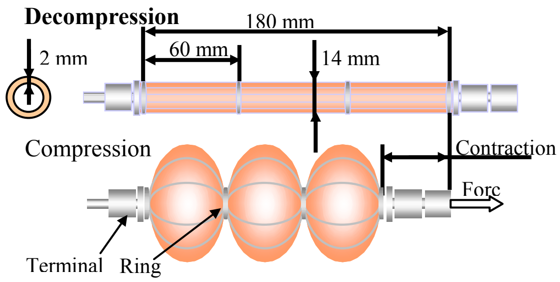

Fig. 1 Straight-fiber-type artificial muscle

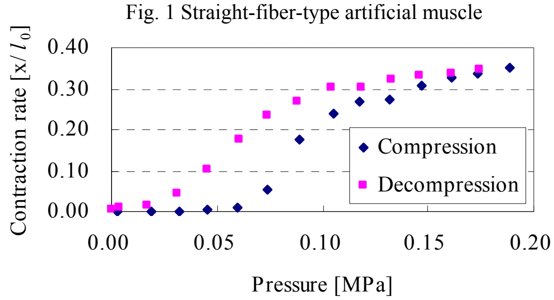

Fig. 2 Relationship between pressure and contraction rate

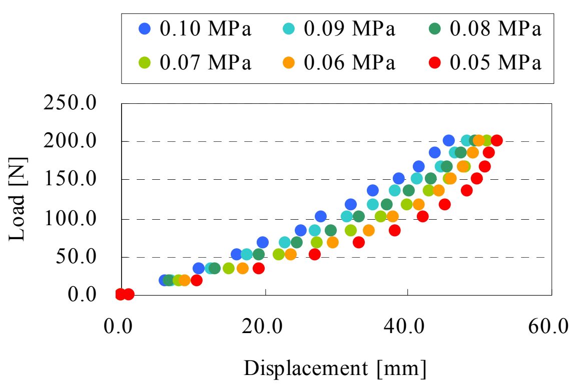

Fig. 3 Relationship between displacement and load.

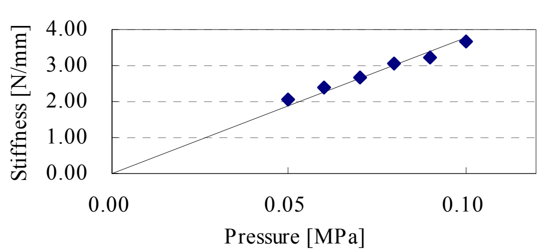

Fig. 4 Relationship between pressure and muscle stiffness

III. 6-DOF MANIPULATOR

A. 6-DOF Manipulator

Fig. 5 shows the manipulator developed in this study. It consists of six joints that create a human-like structure and behavior. The manipulator uses the artificial muscle as an actuator and the muscles are arranged to cover the arm link with an endoskeletal framework. This structure assures safety during the manipulator–human interaction.

Fig. 6 shows a schematic diagram of all of the manipulator joints. Each joint is controlled by two antagonistic muscles, each of which is connected to a proportional solenoid valve. Two artificial muscles are tied with a wire and arranged with a pulley fixed to the joint rotation axis, such that they work in opposition. An initial pressure P_0 is applied to both muscles; In addition $+\Delta P$ is applied to one artificial muscle at the same time as $-\Delta P$ is applied to the other muscle. The difference between the muscles is the contractile force, which is converted into a rotational movement by the pulley, thus driving the joint. The initial pressure P_0 changes the antagonistic force. Fig. 4 shows that the initial pressure changes the joint stiffness, thus joint angles and stiffness can be controlled individually.

B. Kinematics Calculation

It is necessary to compute the extent of displacement of each joint angle in order to make the end effecter of the manipulator take a specific position and configuration. Conversely, it is necessary to calculate the position of the end effecter from the current joint angle, plan the orbit, and use this information for control.

In this study, we carried out direct and inverse kinematics calculations to determine the relationship between each joint angle and the end effecter position and configuration.

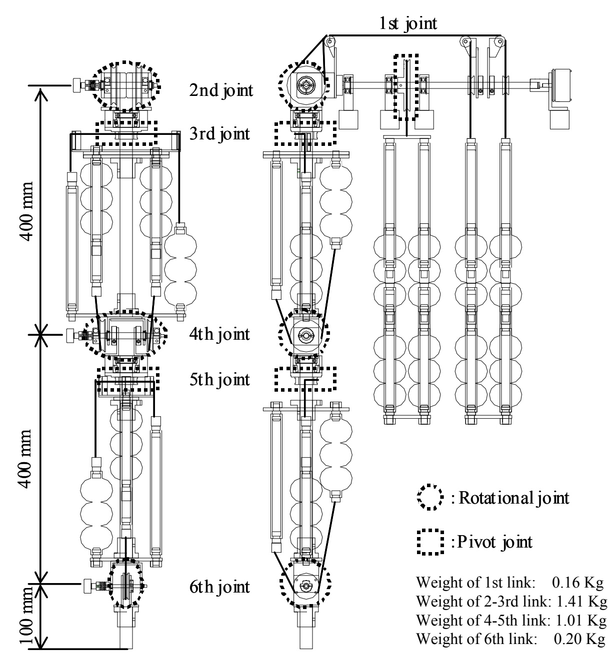

(a) Schematic diagram

(b) Photograph

Fig.5 6-DOF artificial muscle manipulator

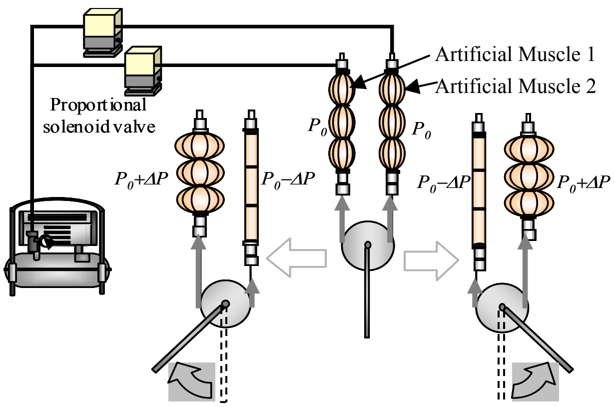

Fig.6 Schematic diagram of a joint

1) Direct Kinematics Calculation

The origin of the standard coordinates is set in the axis of rotation of the second joint. As shown in Fig. 7, $\sum_i$ is the link frame of i joint set within it, l_i the length of the link in i joint, and P the located vector of the end-effecter coordinate.

Table 1 shows the link parameters following the DH notation, where a is the link length, α the angle of a link twist, d the distance between links, and θ the angle between the links.

The homogeneous transformation matrix between the adjoining coordinate systems ${}^{i}T_{i+1}$ is calculated from Table 1. The coordinate system expressing the end-effecter position and posture ${}^{0}T_h$ is derived as shown in Eq. (2).

$$ {}^{0}T_h = \left(\prod_{i=0}^{6} {}^{i}T_{i+1} \right) {}^{6}T_h \qquad (2) $$

where, ${}^{6}T_h$ is the homogeneous transformation matrix between the coordinate system of the sixth joint and the end effecter.

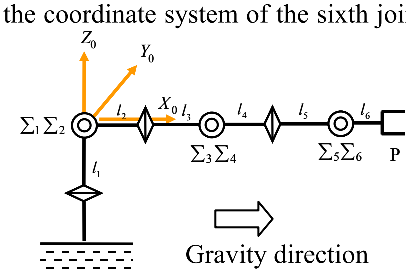

Fig.7 Setting of joint coordinate systems

Table 1 Link parameters.

i	a_{i-1} [deg]	α_{i-1}[deg]	d_i [mm]	θ_i(max) [deg]	θ_i(min) [deg]	l_i [mm]
1	0	0	0	140	-40	0
2	0	90	0	160	0	0
3	0	90	l_2+l_3	90	-90	400
4	0	-90	0	130	0	0
5	0	90	l_4+l_5	90	-90	400
6	0	-90	0	160	0	100

2) Inverse Kinematics Calculation

We calculated each joint angle ϕ_i, from the position and posture of the end effecter, by inverse kinematics calculations. Here, J_i is the joint coordinate vector of $\sum_i$, e_{iy} the directional vector of the axis of rotation of J_i, and e_{ix} the directional vector of the axis of J_i.

Firstly, the end effecter coordinates positional vector P and posture are provided and J_6 is obtained. Further, J_4 is obtained from the point at the intersection of the ball of $l_2 + l_3$ in the radius that centers on J_2 with the circle of $l_4 + l_5$ in the radius that centers on J_6, as shown Fig. 8 and Eq. (3).

$$ \begin{aligned} |J_4|^2 &= (l_2+l_3)^2 \\ |J_6-J_4|^2 &= (l_4+l_5)^2 \\ (J_6-J_4)\cdot e_{6y} &= 0 \end{aligned} \qquad (3) $$

ϕ_1 and ϕ_2 are calculated from the position of J_4 (shown in Fig. 9), ϕ_3 from the angle between e_{2y} and e_{4y}, ϕ_4 from the angle between e_{2x} and e_{4x},ϕ_5 from the angle between e_{4y} and e_{6y}, and ϕ_6 from the angle between e_{4x} and e_{6x}.

By this procedure, the group in each joint angle has eight types of solutions.

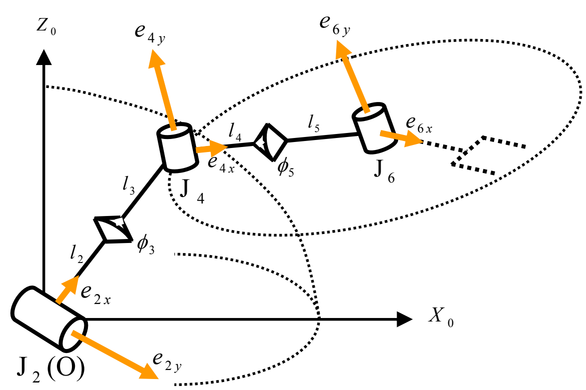

Fig.8 Calculation of inverse kinematics around J_4

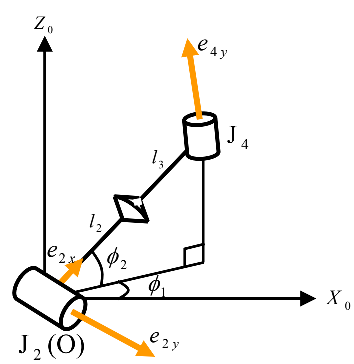

Fig.9 Calculation of ϕ_1 and ϕ_2

C. Control System

1) EQUILIBRIUM MODEL LINEARIZATION

Here we talk about the manipulator control system. This artificial muscle manipulator has a highly nonlinear characteristic, and the gain of the input and output angles is unequal. Due to this unequal gain, position control tends to be unstable. Therefore, we use the mechanical equilibrium model for linearization[8]. The equations of the mechanical equilibrium model are expressed as

$$P_1(\theta_d,\tau)=\left[G_{11}(\phi_{01})G_{22}(\phi_{02})-G_{12}(\phi_{02})G_{12}(\phi_{01})+\frac{K_j}{K_{a2}}G_{21}(\phi_{01})G_{32}(\phi_{02})+\frac{\tau}{r}G_{21}(\phi_{01})G_{22}(\phi_{02})\right]\Big/\left[G_{22}(\phi_{02})G_{31}(\phi_{01})+\frac{K_{a1}}{K_{a2}}G_{21}(\phi_{01})G_{32}(\phi_{02})\right], \quad (4)$$

$$P_2(\theta_d,\tau)=\frac{K_{jd}}{K_{a2}}-\frac{K_{a1}}{K_{a2}}P_1, \quad (5)$$

where

$$\phi_{0i}(x_{di}')=\frac{2\alpha_i l_{0i}^{1.5}x_{di}'^{0.5}}{(l_{0i}-x_{di}')^2+\alpha^2 x_{di}' l_{0i}}, \quad (6)$$

$$G_{1i}(\phi_{0i})=\frac{4K_i t_i}{d_{0i}}\left[\frac{l_{0i}}{d_{0i}}\right]^2\left[\frac{\sin\phi_{0i}-\phi_{0i}\cos\phi_{0i}}{\phi_{0i}^2}\right], \quad (7)$$

$$G_{2i}(\phi_{0i})=\frac{M\tan\phi_{0i}}{d_{0i}nbi}, \quad (8)$$

$$G_{3i}(\phi_{0i})=2\left[\frac{l_{0i}}{d_{0i}}\right]\left[\frac{\phi_0-\sin\phi_{0i}\cos\phi_{0i}}{\phi_{0i}^2}\right]+4\frac{l_{0i}}{d_{0i}}\frac{\sin\phi_{0i}}{\phi_{0i}}-\frac{M\pi d_{0i}}{nb_i}\tan\phi_{0i}. \quad (9)$$

$$x_{d1}'=\frac{r\psi_1-r\theta_d}{3}, \quad (10)$$

$$x_{d2}'=\frac{r\psi_2+r\theta_d}{3}. \quad (11)$$

If the joint angle, θ, has the target value, θ_d, then pressures P_1 and P_2, given by (4) and (5), are the pressure values needed to realize the target value, θ_d. Therefore, θ, and θ_d have a linear relationship. Here torque is fed back to those equations. In this study, these compensations are called as equilibrium model linearization (EML). By inputting a desired value K_{jd}, joint stiffness K_j can be controlled, which further controls the effect of inertia and load torque. If stiffness characteristic constant K_{a1}, K_{a2} are equal, relationship between joint stiffness K_j and initial pressure P_0 is proportional. So we can select desirable joint stiffness or average pressure method.

Fig. 10 shows a block diagram of the EML. Fig. 11 shows the experimental results of position control using the EML as a parameter of joint stiffness. Although some errors may be observed in this figure, it has sufficient line linearization. Fig. 12 shows the experimental results of joint stiffness. Joint stiffness is measured with a constant desirable angle and variable joint stiffness and load torque. Although the figure shows some errors, we can select the approximate joint stiffness.

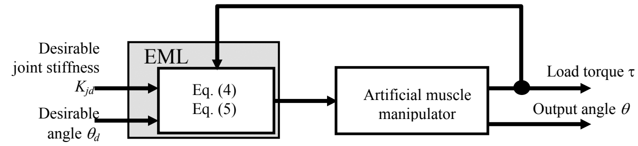

Fig. 10 Block diagram of the feed-forward control of the joint.

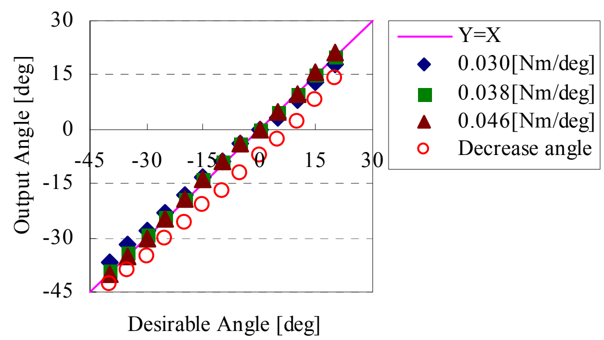

Fig. 11 Comparison of desirable curve and experimental results of joint angle as parameter of compliance

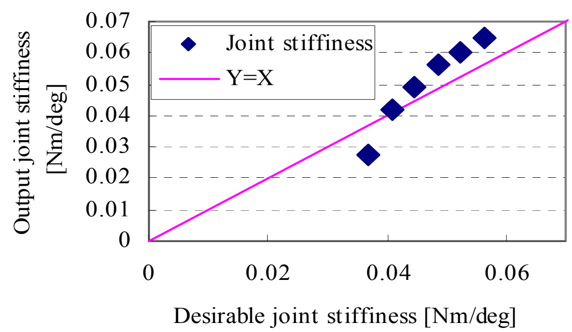

Fig. 12 Comparison of the desired curve and experimental results of EML of joint stiffness.

2) FEEDBACK CONTROL SYSTEM

This artificial muscle manipulator can be controlled by EML, but errors result from inaccuracies in the mechanical equilibrium model and due to the hysteresis characteristics. The dynamic characteristics of EML, as parameters of the desired position, are almost constant. Therefore, we introduce PI control, to the EML position feedback, so that it compensates for the positional errors. Thus, we control the manipulator by both EML and PI control.

The block diagram of the position control is shown in Fig. 13, where x, y, and z are the position, ϕ, θ, and ψ the configurations of the end effecter, θ_{di} the desired angle of each joint, and θ the measured angle. We applied inverse kinematics to convert (x, y, z) and (ϕ, θ, ψ) into θ_{di}. The proportional gain and integral gain of the PI controller are constant values set by the cut-and-try method. The load torques from each joint is fed back to the EML for torque compensation.

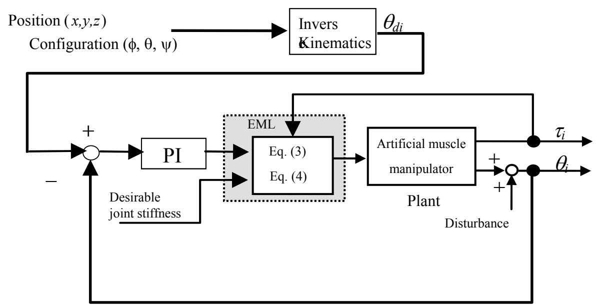

Fig. 13 Block diagram of position control system of the manipulator.

IV. Experiment

In order to evaluate the stability of the manipulator, we executed two experiments on position control. Experiment 1 compared the controller stability between the proposed method and conventional PI control. Experiment 2 evaluated the disturbance rejection by compliance control. Both experiments used the same desired positions, as shown in Table 2.

We used two video cameras to measure the end effecter position, placed at right angles to each other, with one recording in the x-y plane and the other in z-x plane. After recording, the end effecter position was measured by analyzing the two movies using the Movias Pro (NAC Image Technology) operating analysis software.

Table 2 Target position and configuration

(a) Initial value

x	0.00 [m]
y	0.00 [m]
z	0.00 [m]
θ	0 [deg]
ϕ	0 [deg]
ψ	0 [deg]

(b) Desired value

x	0.55 [m]
y	0.30 [m]
z	0.50 [m]
θ	125 [deg]
ϕ	-70 [deg]
ψ	-115 [deg]

A. Experiment 1 (Comparison of the proposed method with PI control)

Figs. 14 and 15 show the experimental results of position and control signal comparison between the proportional and conventional PI control and the open loop control (feed forward control).

As shown in Fig. 14, feed forward control has some error, caused by model accuracy and hysteresis, associated with it. On the other hand, PI feedback controls converge in the desired position. This demonstrates that manipulator position control is possible with the introduction of PI feedback control. Fig. 15 shows that the response of the proposed method is faster than the conventional PI control. On the contrary conventional PI control uses a larger control signal than the proposal method. This means that the proposed method reduces load on the control system, by taking into account the nonlinear characteristics of the manipulator, which is more stable than the conventional PI control.

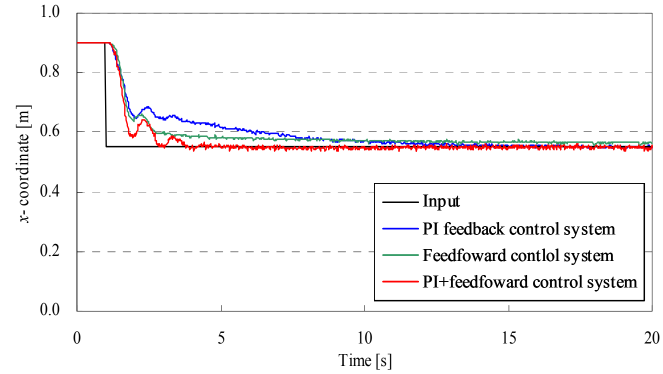

(a) x-coordinate

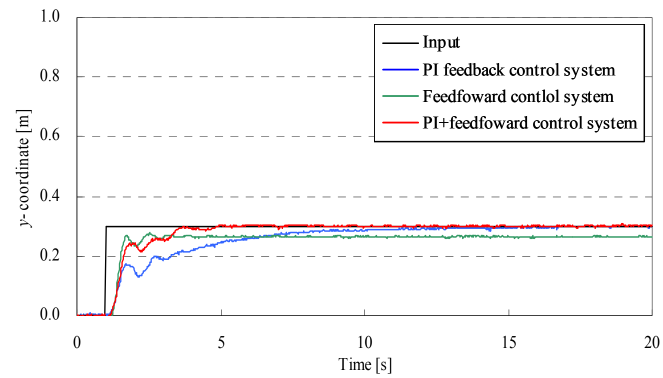

(b) y-coordinate

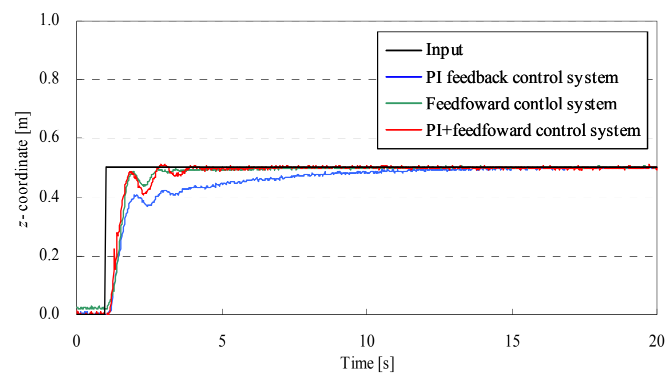

(c) z-coordinate

Fig.14 Experimental result of position control (z-coordinate)

B. Experiment 2 (Disturbance rejection by compliance control)

Fig. 16 shows the experimental results of comparison of position control with various initial pressures P_0. In this experiment, we fixed a weight (0.5 kg) on the manipulator end effecter. The controller was then proposed as a method of PI + feed forward control.

A high initial pressure provides more stability than low initial pressure. This means that the robustness of the manipulator to disturbance torque can be changed by changing the initial pressure, which is independent from the position control system. Also, an appropriate compliance adapting manipulator for the environment can be selected.

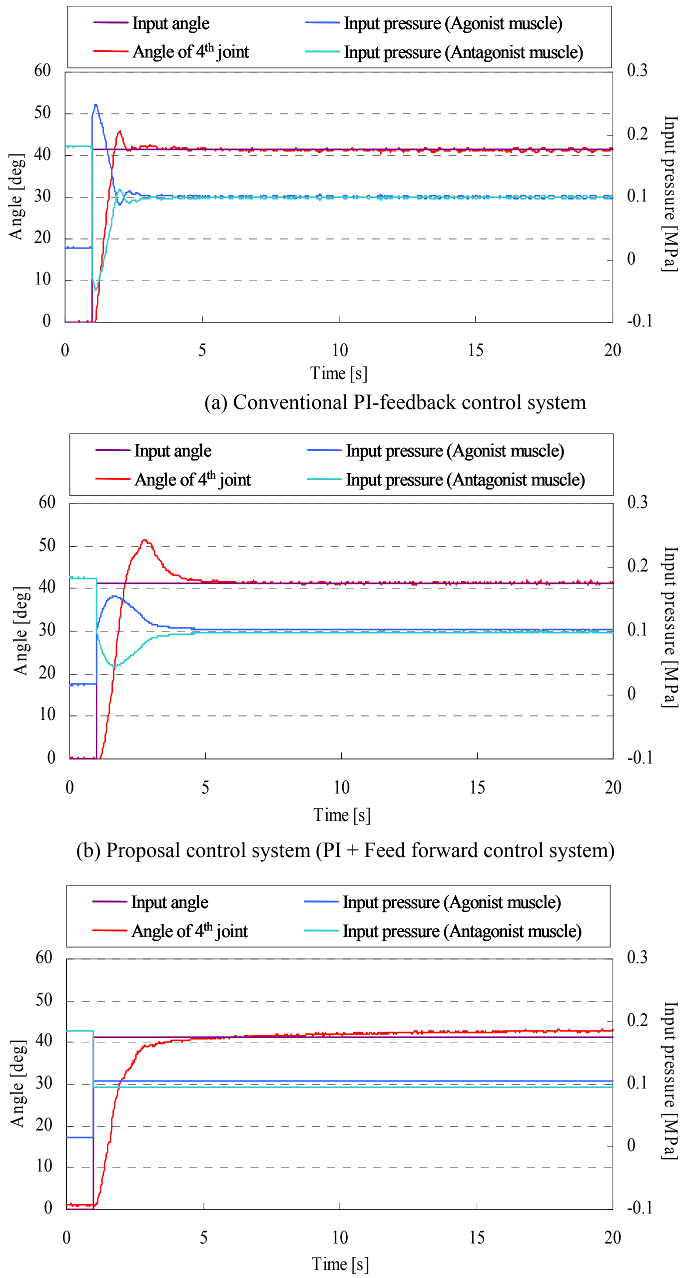

(a) Conventional PI-feedback control system

(b) Proposal control system (PI + Feed forward control system)

(c) Feed forward control system

Fig.15 Experimental comparison between the joint behavior and input pressure in the fourth joint.

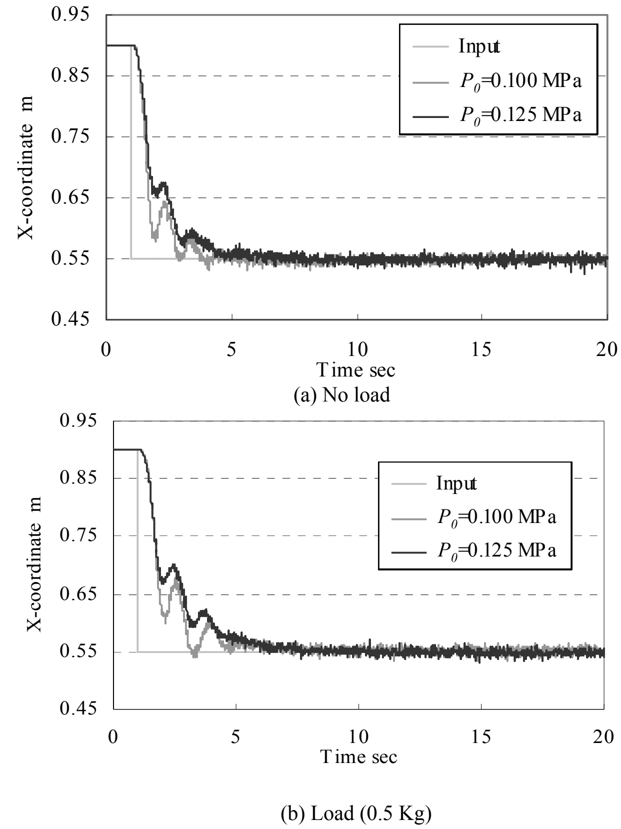

(a) No load

(b) Load (0.5 Kg)

Fig. 16 Experimental result of position control for each initial pressure (x-coordinate).

V. Conclusion

In this study, we developed a 6-DOF artificial muscle manipulator and considered a stable position control method. Our results were as follows:

1. We developed a 6-DOF artificial muscle manipulator based on human arm and carried out kinematics calculations for end effecter position control.
2. PI control was used to compensate for the displacement angles.
3. The mechanical equilibrium model with an artificial muscle manipulator produced a good linear relationship and reduced the controller load.
4. Applying the proposed joint stiffness control to the manipulator changed the manipulator disturbance rejection.

References

[1] T. Nakamura, N. Saga, and K. Yaegashi, "Development of Pneumatic Artificial Muscle based on Biomechanical Characteristics," in Proc. IEEE International Conference on Industrial Technology (ICIT 2003), 2003, pp. 729–734.

[2] V. L. Nickel, M. D. J. Perry, and A. L. Garrett, " Development of useful function in the severely paralysed hand," Journal of Bone and Joint Surgery 45A(5), 1963, pp. 933–952

[3] M. M. Gavrilovic and M. R. Maric, "Positional servo-mechanism activated by artificial muscles," Medical and Biological Engineering 7, 1969, pp. 77–82.

[4] G. K. Klute, J. M. Czernieki, and B. Hannaford, "McKibben Artificial Muscles: Pneumatic Actuators with Biomechanical Intelligence," Proceedings of the IEEE/ASME International Conference on Advanced Intelligent Mechatronics 1999, pp. 221–226.

[5] C. P. Chou and B. Hannaford, "Static and Dynamic Characteristics of McKibben Pneumatic Artificial Muscles," Proceedings of IEEE International Conference On Robotics and Automation 1994, pp. 281–286.

[6] T. Nakamura, "Experimental Comparisons between McKibben type Artificial Muscles and Straight Fibers Type Artificial Muscles," SPIE International Conference on Smart Structures, Devices and Systems III, 2006

[7] [7] T. Nakamura and H. Shinohara, "Position and Force Control Based on Mathematical Models of Pneumatic Artificial Muscles Reinforced by Straight Glass Fibers," Proceedings of IEEE International Conference on Robotics and Automation (ICRA 2007) 2007, pp. 4361–4366

[8] T. Nakamura, H. Maeda, H. Nagai, and H. Saito, " Position and compliance control of an artificial muscle manipulator using a mechanical equilibrium model," in Proc. Annual Conference of the IEEE Industrial Electronics Society (IECON 2008), Digital Object Identifier 10.1109/IECON.2008.4758512.